Quaternary Research 82 (2014) 354–365

Contents lists available at ScienceDirect

Quaternary Research

journal homepage: www.elsevier.com/locate/yqres

Overbank flooding and human occupation of the Shalongka site in the Upper Yellow River Valley, northeast Tibet Plateau in relation to climate change since the last deglaciation

Guoqiang Li, Guanghui Dong *, Lijuan Wen, Fahu Chen

Key Laboratory of Western China's Environmental Systems, Ministry of Education, Research School of Arid Environment and Climate change, Lanzhou University, Lanzhou 730000, China

ARTICLE INFO

Article history:
Received 6 February 2014
Available online 20 August 2014

Keywords:
Upper Yellow River
Overbank flooding
OSL dating
^{14}C dating
Human occupation
Prehistoric period

ABSTRACT

Increased flooding caused by global warming threatens the safety of coastal and river basin dwellers, but the relationship of flooding frequency, human settlement and climate change at long time scales remains unclear. Paleolithic, Neolithic and Bronze Age cultural deposits interbedded with flood sediments were found at the Shalongka site near the north bank of the upper Yellow River, northeastern Tibetan Plateau. We reconstruct the history of overbank flooding and human occupation at the Shalongka site by application of optically stimulated luminescence and radiocarbon dating, grain size, magnetic susceptibility and color reflectance analysis of overbank sediment and paleosols. The reliability of OSL dating has been confirmed by internal checks and comparing with independent ^{14}C ages; alluvial OSL ages have shown a systematic overestimation due to poor bleaching. Our results indicate that the Yellow River episodically overflowed and reached the Shalongka site from at least ~16 ka and lasting until ~3 ka. Soil development and reduced flooding occurred at ~15, ~8.3–5.4, and after ~3 ka, and prehistoric populations spread to the Shalongka site area at ~8.3, ~5.4, and ~3 ka. We suggest that climate change influenced the overbank flooding frequency and then affected prehistoric human occupation of the Shalongka site.

Introduction

Rise in global average temperature is already causing extreme weather events and increasing risk of flooding is beginning to affect the lives of millions (Min et al., 2011; Pall et al., 2011; IPCC, 2012). The increasing intensity and frequency of flooding in the valleys of rivers around the world pose a great threat to the safety of humans nearby (Wilby et al., 2008; Botzen and Van Den Bergh, 2009; de Moel et al., 2009; Milly et al., 2002). Prehistoric people favored settlement near river valleys in order to obtain water and subsistence resources, making them vulnerable to flooding disasters, as much as or even more than at present. Thus, the exploration of dynamic relationships between flooding and human settlement near rivers on a long term scale is of significance, and can provide perspectives on human settlement and climatic changes in areas subject to frequent flooding.

The linkages between climate change, floods and human settlements on different reaches of rivers in China have been often studied (e.g., Yang et al., 2000, 2003; Huang et al., 2010; Dong et al., 2013a; Ma et al., 2014), and it has been suggested that variable and unstable climates typified by flooding and/or droughts may have resulted in settlement destruction and abandonment. For example, the Lajia Site, a Qijia Culture site (4100–3600 cal yr BP) located in the Guanting Basin near the upper reaches of the Yellow River, was ruined by contemporary earthquakes and floods (Yang et al., 2003). Paleoflood disasters in the Guanting Basin occurred between 6500–2220 cal yr BP and influenced human settlements during that period (Hou et al., 2012; Ma et al., 2014). One of these events may have been caused by the breaching of a large dammed lake in the upper reaches of the Yellow River (Dong et al., 2014) caused by variation in monsoon precipitation (Ma et al., 2014).

The Jinghe River is a tributary of the middle reaches of the Yellow River, and extraordinary floods and droughts along the river related to abrupt climatic shifts between 4200–4000 cal yr BP resulted in settlement abandonment, and the possible decline of highly developed late Neolithic civilizations in China's monsoonal regions (Huang et al., 2010). The collapse of late Neolithic urban centers of the Longshan culture (4350–3950 cal yr BP) in the lower reaches of the Yellow River, and the Liangzhu culture in the lower reaches of the Yangtze River, have been attributed to great floods (Wang et al., 2005; Gao et al., 2007). Also in the lower Yellow River, the Sanyangzhuang site (~2100 cal yr BP) on the North China plain was inundated by a sudden burst of muddy water from a catastrophic levee breach during the late Western Han period (~202 BC–AD 9). There was apparently little warning as workers reroofing one compound left behind their tools and tiles (Kidder et al., 2012a,b). However, these previous studies have mainly focused on reconstruction of hydrological/

* Corresponding author.
E-mail address: ghdong@lzu.edu.cn (G. Dong).

http://dx.doi.org/10.1016/j.yqres.2014.07.005
0033-5894/

cultural relationships during short episodes (e.g., Yang et al., 2000, 2003; Huang et al., 2010), while relationships among flood disasters, human settlement and climate change at long time scales are still poorly understood.

The Yellow River is located in a semi-arid region of China and is characterized by a marked flood frequency (Yang et al., 2000). As recorded in Chinese history, the Yellow River broke through its levees 1593 times with 26 major changes of course in the past 2550 years, an average of two breaches every 3 years and one major course change per century (YRCC, 1959). Paleofloods occurred frequently along the upper Yellow River during the Holocene, and at least 4 cycles of frequent flooding followed by periods of reduced flooding have been detected (Ma et al., 2014). Hundreds of prehistoric archeological sites have been found in the upper valleys of the Yellow River (BNCR, 1996; Aldenderfer, 2006; Dong et al., 2013a) and are mainly distributed on adjacent river terraces. Cultural layers sandwiched between paleoflood sediments are present in many of these valley basins (Dong et al., 2013a; Ma et al., 2014) and provide sedimentological records with which to explore relationships between ancient human occupation and flooding-related environment change.

Radiocarbon dating is the most commonly used method for establishing chronologies of archeology sites, which has been widely applied to the archeology sites on Tibet Plateau (e.g., Sun et al., 2010, 2012; Dong et al., 2013a). However, the ^{14}C method can be problematic in dating eolian deposits because of their low organic carbon content (Li et al., 2007), and dates on organic carbon from sediment of archeology sites are often overestimated because of a reservoir effect (Björck et al., 1991; Colinan et al., 1996; Wang et al., 2002b). OSL dating technology can determine the ages of eolian and waterlain deposits by directly measuring quartz or feldspar minerals (Aitken, 1998). With the development of the single-aliquot regenerative-dose (SAR) protocol (Murray and Wintle, 2000), quartz OSL dating is now being widely applied to the dating of Quaternary sediments in Tibet Plateau and other parts of northwestern China (Zhao et al., 2007; Lai et al., 2009; Zhang et al., 2012; Zhao et al., 2012; Han et al., 2014; Lai et al., 2014; Yu and Lai, 2014). In the Tibet plateau, OSL dating also has been successfully applied to the Xindian Culture site of Lamafeng on the NE edge of the Tibetan Plateau, where OSL ages have shown a good consistence to the charcoal accelerator mass spectrometry (AMS) dating ages of culture layer (Hou et al., 2012). Sun et al. (2010) dated the archeological sites in Xiao Qaidam Lake of the NE Tibetan Plateau by quartz OSL dating, and OSL ages provide the time frame for this archeological site which ranges from ~3 to 11 ka.

The Shalongka (SLK) archeology site is located on second terrace of the upper Yellow River valley in the Qunjian Basin, northeastern Tibetan Plateau (TP) (Figs. 1a, b). Artifacts representative of Paleolithic, Majiayao (5900–4000 cal yr BP) and Kayue (3400–2600 cal yr BP) cultural periods, as well as overbank deposits were found in a stream cut exposure (BNCR, 1996; Dong et al., 2013a). As a kind of fluvial process, overbank floods have often left their sedimentary records over the inundated areas in their paths. Overbank floods deposit was the suspended sediment load in floodwater flow and deposited in areas of flow separation and has been preserved after the flood recession (Huang et al., 2010). Some culture layers occur in paleosol layers interbedded in Yellow River overbank flood deposits (Fig. 2).

In this study, ^{14}C dating methods were employed to determine the ages of these culture layers and associated paleosols. OSL dating methods were applied to eolian and fluvial deposit by directly measuring quartz minerals, and a quartz single-aliquot regenerative-dose protocol was tested by the use of internal checks and equivalent dose (D_e) determinations. In the following, the reliability of OSL dating applied to potentially poorly bleached flooding deposit is discussed in comparison to independent ^{14}C dating ages and reliable eolian quartz ages. By combining the lithology, chronology, and proxy indexes of grain size, magnetic susceptibility and color reflectance analysis and comparing the results with high-resolution paleoclimatic records, we identify periods of Yellow River overbank flow at the SLK site since the last deglaciation and discuss the relationship between human settlement and changing climatic conditions.

Materials and methods

Study area, section and sampling

The upper Yellow River valley is situated in the northeastern TP. The Guanting, Xunhua-Hualun and Qunjian basins are distributed from southeast to northwest along the Yellow River. As shown in Figure 1B, the Qunjian Basin is surrounded by Songba Gorge (east), Gongbo Gorge (west), Laji Mountains (north) and Geji Mountains (east). The Yellow Rivers runs through the western part of the basin from NW to SE. The basin has a annual average temperature of 7.8°C, and annual average precipitation of 357.3 mm with 70% of that precipitation occurring during the summer. Elevations range between 1960 and 4614 m, and the Yellow River drops from 2020 m a.s.l. in the northwest to 1990 m in the southeast.

The SLK site (36.01°N, 102°E, 2021 m) is located on the second terrace of the Yellow River in the southern Qunjian Basin, ~500 m north of the present Yellow River channel. It consists of three paleosol layers interbedded in Yellow River overbank deposits. A microlithic cultural layer is present in the bottom of the middle paleosol layer. As shown in Figure 2, nine OSL samples and five ^{14}C samples were collected from the SLK site for chronological determinations. OSL samples SLK-126-130, SLK-190-194 and SLK-270-274 were collected from 126 to 136 cm, 190 to 194 cm, and 270 to 274 cm in the paleosol layers, while samples SLK-36-40, SLK-92-96, SLK-160-164, SLK-216-220, SLK-256-260, and SLK-320-324 were collected at depths of 36–40 cm, 92–96 cm, 160–164 cm, 216–220 cm, 256–260 cm, and 320–324 cm in fluvial silty sand. For ^{14}C dating, charcoal sample SLK-01 was collected from a Kayue cultural layer at 10 cm near the surface. Two bulk organic matter samples SLK-02 and SLK-03 were collected from depths of 115 cm and 180 cm in the middle paleosol, and two charcoal samples, SLK-04 and SLK-05, were collected at depths of 180 cm and 190 cm of the lowest culture layer. Bulk samples at 2-cm intervals were collected from the entire 320-cm section for environmental proxy analysis.

OSL dating and ^{14}C dating

OSL dating sample preparation and measurement

All laboratory sample preparation and luminescence measurements were carried out in a darkroom with subdued red light. All raw samples were treated with 10% HCl and 20% H_2O_2 to remove carbonate and organic matter. The samples were then sieved in water to select sediments consisting of grains with specific sizes of 90–150 μm. Heavy liquids with densities of 2.62 g/cm^3 and 2.75 g/cm^3 were then used to separate quartz and feldspar fractions of each sample. Quartz grains were treated with 40% HF for 60 min to remove the outer layer that was irradiated by alpha particles and any remaining feldspar grains. Then, all samples were treated with 1 mol/L HCl for 10 min to remove fluorides created during the HF etching.

OSL signals were measured using an automated Risø TL/OSL-DA-15 reader (Markey et al., 1997). The OSL signal was detected through two 3-mm-thick Hoya U-340 filters. Laboratory irradiation was carried out using $^{90}Sr/^{90}Y$ sources mounted within the reader, with a dose rate of 0.104 Gy/s. The purity of quartz extracts was verified using infrared stimulation. For the quartz grains, in order to eliminate the influence from feldspar contamination, the post-IR single aliquot regenerative protocol (SAR) was employed to measure D_e values from quartz extracts in 5-mm aliquots (Banerjee et al., 2001; Zhang and Zhou, 2007).

https://doi.org/10.1016/j.yqres.2014.07.005 Published online by Cambridge University Press

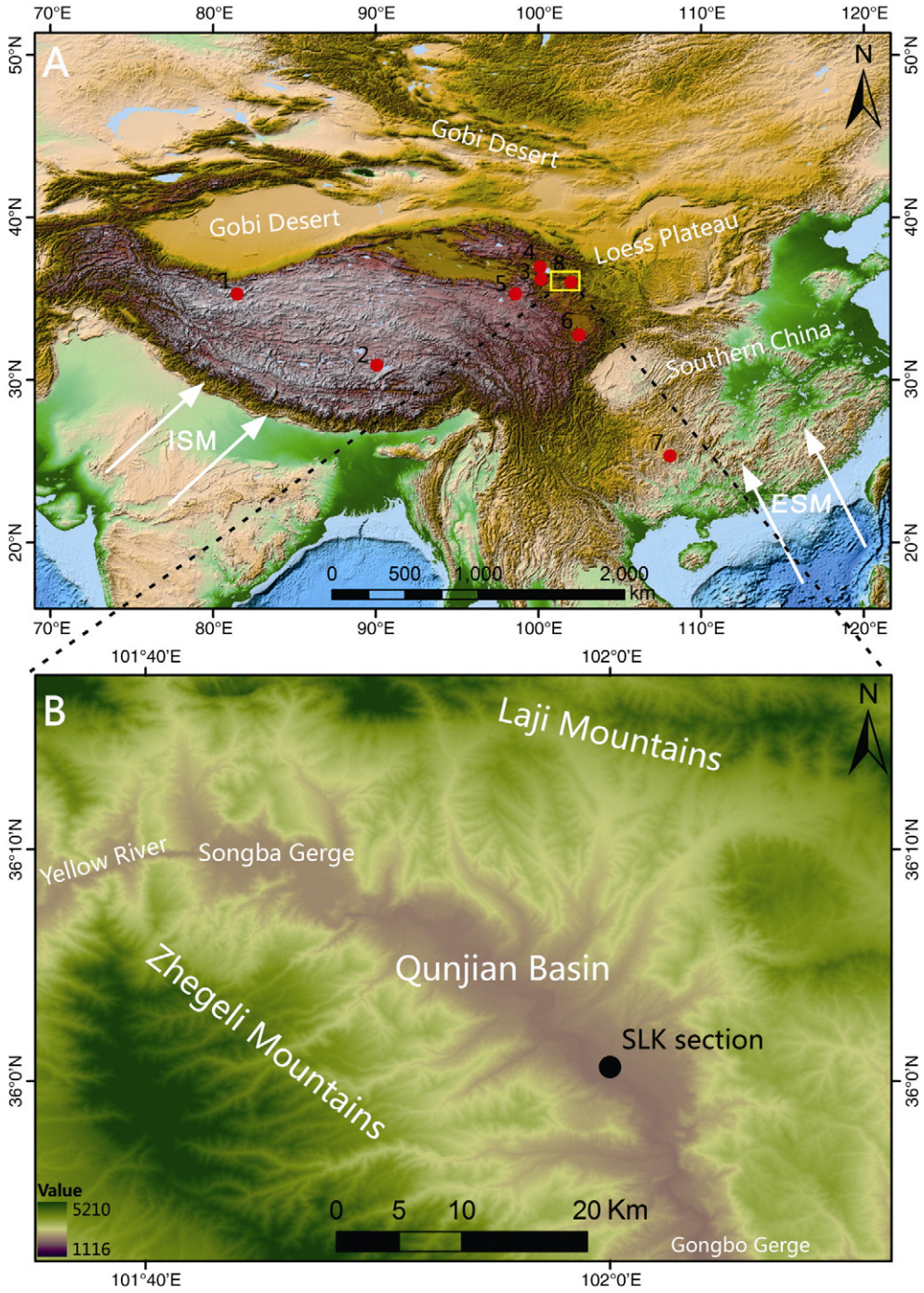

Figure 1. The location of study area and other localities mentioned in the text (Fig. 1A): 1—Guliya ice core; 2—Tianmen Cave; 3—Qinghai Lake; 4—Genggahai Lake; 5—Dongji Cona Lake, 6—Hongyuan peatland; 7—Dongge Cave; and 8—SKL site. Fig. 1B shows the location of the Qunjian basin and the SLK site locality.

The environmental dose rate was calculated from the measurements of radioactive element contents in the sample and surrounding sediments, with a small contribution from cosmic rays. For all samples, the uranium (U) and thorium (Th) concentrations and potassium (K) content were determined by means of Neutron Activation Analysis (NAA). All results were converted to beta and gamma dose rates according to the conversion factors of Aitken (1998). The dose rate from cosmic rays was calculated according to sample burial depth and the altitude of the section (Prescott and Hutton, 1994). Water content may change drastically after burial for those samples that were collected from lacustrine sediments in an arid area. Due to the uncertainty of sediment water content in the burial period, a water content of 5 ± 2.5% and 10 ± 5% was introduced to calculate ages for eolian sand and fluvial sediment, respectively.

^{14}C dating sample measurement

Charcoal samples SLK-01 and SLK-04, and bulk organic matter samples SLK-02 and SLK-03 were dated using the conventional liquid scintillation counting method at the MOE Key Laboratory in Lanzhou University. The IntCal09 curve (Reimer et al., 2009) and the Libby half-life of 5568 years were used in the calculation of all dates, with the calibration performed using Calib (v.6.0.1) (Stuiver and Reimer, 1993). All ages reported are relative to AD 1950 (referred to as "cal yr BP").

https://doi.org/10.1016/j.yqres.2014.07.005 Published online by Cambridge University Press

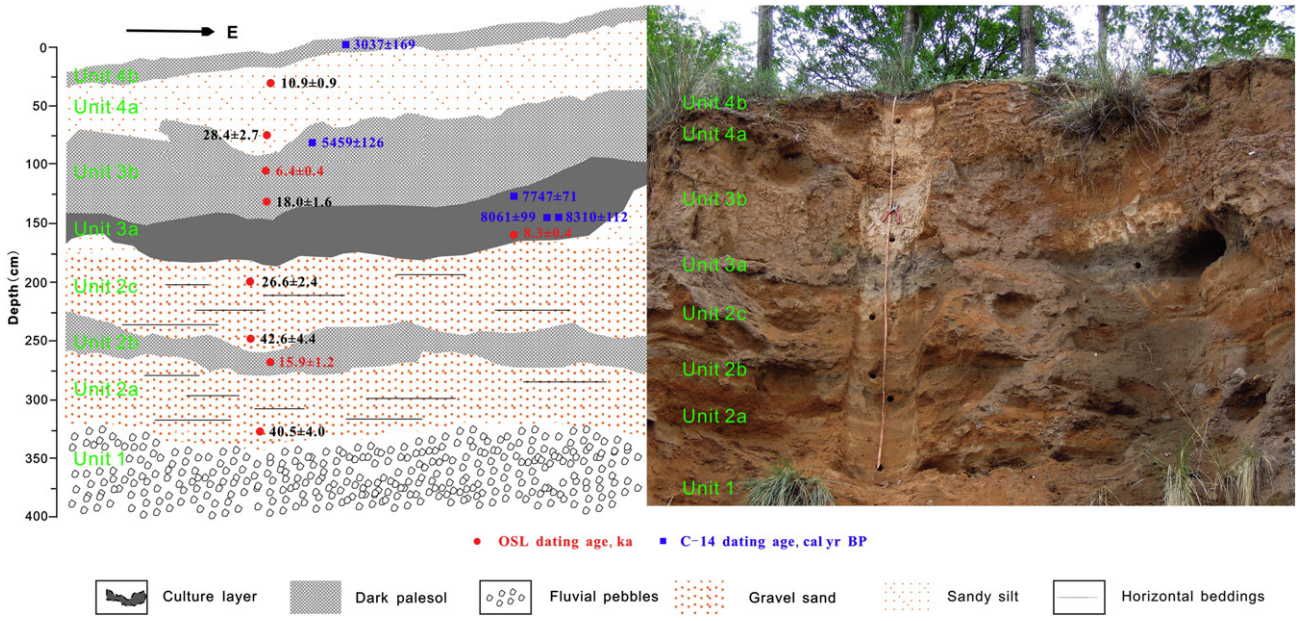

Figure 2. Lithology, photo, and dating results for the SLK section. All of the OSL ages are labeled besides the red circles. The OSL ages in red are reliable OSL ages and are used for chronology; the OSL ages in black are overestimated OSL ages that were not used for chronology.

Grain size, magnetic susceptibility and color reflectance analysis

A total of 165 grain-size samples from SLK section, collected at intervals of 2 cm, were measured. The samples were pretreated with 10 ml of 30% H_2O_2 to remove organic matter and then 10 ml 10% HCl with heating to remove carbonates. Deionized water was then added and each sample suspension was kept for 24 h to remove acidic ions. Finally, the sample residue was dispersed with 10 ml of 0.1 mol/L $(NaPO_3)_6$ using an ultrasonic vibrator for 10 min to facilitate dispersion (Peng et al., 2005). The grain size was measured using a Malvern Master Sizer 2000 at Lanzhou University. The measurement range is 0.02 and 2000 μm and the mean measurement error is <2%.

The magnetic susceptibility of all 165 samples from the SLK section was determined using 7 g of ground sediment and a Bartington MS2 magnetic susceptibility meter (0.47/4.7 kHz). Color reflectance for these samples was measured using a handheld Minolta-CM2002

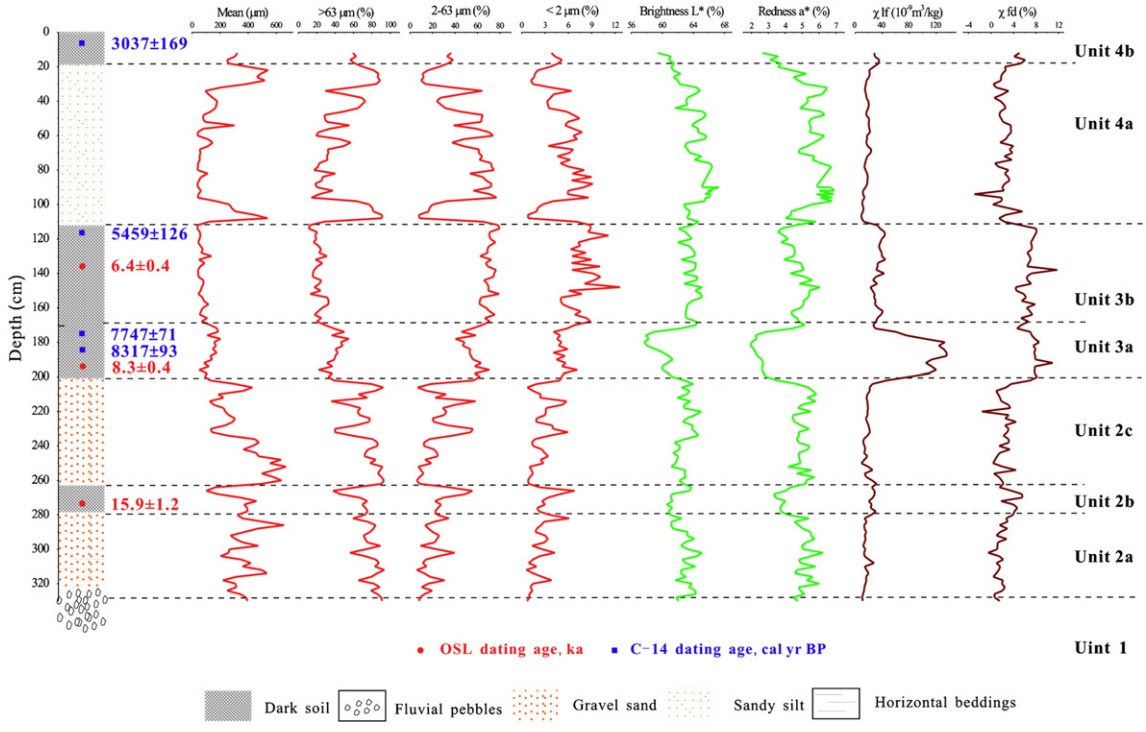

Figure 3. Stratigraphic subdivisions, ages and environmental proxy analyses results for the SLK section.

https://doi.org/10.1016/j.yqres.2014.07.005 Published online by Cambridge University Press

spectrophotometer after a 2–3 g sample was dried at 40°C for 24 h and crushed. The color reflectance values of all samples are given by the spherical L*a*b* color space (Robertson, 1977). Red–green chromaticity a*(+a* is the red direction, −a* is the green direction) and L* (the range from 0 to 100 represents the variations in lightness from black to white).

Results

Lithology

The detailed stratigraphic lithology of SLK section can be divided to four units (Fig. 3).

Unit 4: 0–110 cm, fluvial light brownish-red sandy silt with an uncompacted texture. The top 20 cm is the modern soil layer, containing abundant bio-pores.

Unit 3: 110–210 cm, eolian sandy silt containing paleosol and culture layer intervals. The upper portion of this unit (110–135 cm) is eolian gray sandy silt with soil development. It is firm, compact, breaks into a blocky structure, and is rich in organic matter. The middle 135–170 cm is fluvial brown sandy silt interrupted by a 1–2 cm deep gray soil layer; the bottom 170–210 cm of this unit is a 40-cm cultural layer containing microlithic artifacts including a chalcedony microblade and a chert flake. This layer contained no pottery or other Neolithic remains, and is assumed to be pre-Neolithic pending complete excavation (Dong et al., 2013a).

Unit 2: 200–320 cm, this unit is fluvial brown silty sand with horizontal bedding, interrupted by eolian sandy silt at 263–280 cm. Gravelly coarse sand irregularly occurs at 240–250 cm.

Unit 1: >320 cm, sandy gravel of the second terrace of the Yellow River.

Chronology

OSL dating results

The suitability of the quartz SAR sequence for D_e determination was checked with a 'dose recovery test' (Murray and Wintle, 2003) for sample SLK-190-194. This test examines the combined function of all the conditions of the procedure, such as preheat temperature, size of test dose, etc. The sample was prepared into 6 groups with 4 aliquots for each group. Preheat temperatures from 220°C to 300°C at 20°C intervals for 10 s were tested and the cut-heat was 220°C for 10 s, using a heating rate of 5°C/s. The calculated D_e, recuperation and recycling ratios are plotted in Figure 4a. They indicate that the D_e values are independent of preheat temperature in the range of 220–300°C and a D_e cluster appeared at temperatures of 240–280°C. All the recycling ratios are between 0.9 and 1.1. The recycling ratio for different measurement temperatures is between 1.00 and 1.09. The recuperations for different preheat temperatures were less than 5%, ranging from 0.3 to 1.3%, with the cluster recuperation at 220°C and 260°C. Based on these results the SAR sequence with a preheat temperature of 260°C and a cut-heat of 220°C was selected to measure the D_e of the quartz fraction in our study samples.

As shown in Fig.4b, the OSL signal of nature and regeneration dose decreased very quickly during the first second stimulation, which indicates that the OSL signal is fast-component dominant and the growth curve can be readily fitted using a single saturation exponential (Fig. 4c). For each sample at least twenty aliquots were measured. The D_e and the associated standard error for each sample is listed in Table 1. The extent of OSL sample bleaching was detected and estimated by the scatter patterns of D_e values in radial plots (Galbraith et al., 1999). We observed from Figure 5 that most aliquots of samples SLK-126-130, SLK-190-194 and SLK-270-274 were inside the ±2 standard deviation band in the radial plot, and only few aliquots were outside this band. These imply that the grains in the three eolian samples were well

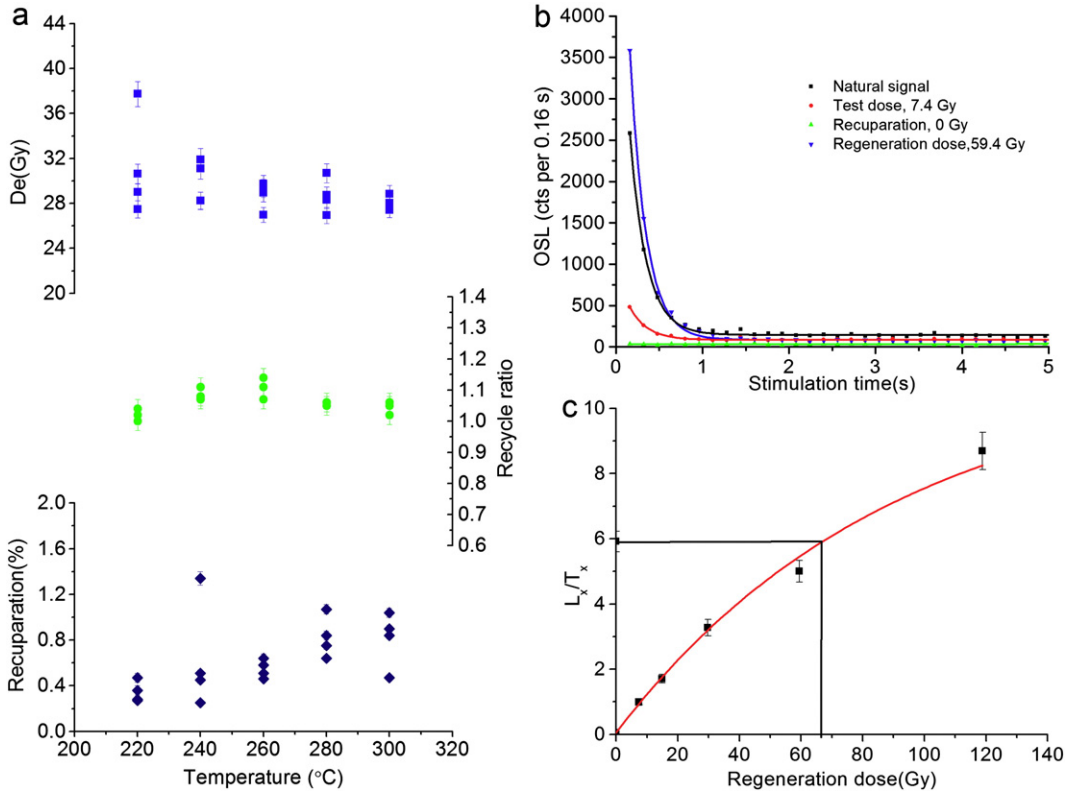

Figure 4. (a). Dose recovery test results for sample SLK-126-130. (b). Luminescence characteristics of sample SLK-270-274: quartz OSL shine-down curves for the natural signal, test dose of 7.4 Gy, and regeneration doses of 59.4 Gy and 0 Gy. The curve of 0 Gy shows that recuperation is negligible. (c). Best fit growth curves for sample SLK-270-274 using an exponential function.

https://doi.org/10.1016/j.yqres.2014.07.005 Published online by Cambridge University Press

Table 1
OSL dating results for samples from the SLK section.

Sample	Aliquots	De (Gy)	Grain size	U (ppm)	Th (ppm)	K (%)	Water content (%)	Cosmic ray (Gy/ka)	Dose rate (Gy/ka)	Age (ka)
SLK-36-40	24	40.92 ± 1.83	90–125	3.31 ± 0.12	8.91 ± 0.28	2.36 ± 0.07	10 ± 5	0.29	3.75 ± 0.25	10.92 ± 0.88
SLK-92-96	24	93.12 ± 6.37	90–125	3.00 ± 0.11	9.46 ± 0.28	1.90 ± 0.06	10 ± 5	0.27	3.29 ± 0.22	28.35 ± 2.72
SLK-126-130	**23**	**26.00 ± 0.62**	**63–90**	**4.03 ± 0.13**	**12.00 ± 0.34**	**2.02 ± 0.06**	**5 ± 2.5**	**0.26**	**4.06 ± 0.20**	**6.41 ± 0.36**
SLK-160-164	23	65.37 ± 4.11	125–180	3.49 ± 0.12	12.30 ± 0.34	2.02 ± 0.06	10 ± 5	0.25	3.63 ± 0.24	18.01 ± 1.64
SLK-190-194	**20**	**30.64 ± 0.52**	**90–125**	**3.47 ± 0.12**	**10.00 ± 0.29**	**1.98 ± 0.06**	**5 ± 2.5**	**0.24**	**3.68 ± 0.16**	**8.32 ± 0.38**
SLK-216-220	20	97.06 ± 5.74	90–125	3.42 ± 0.12	10.40 ± 0.30	2.18 ± 0.06	10 ± 5	0.23	3.65 ± 0.25	26.57 ± 2.39
SLK256-260	24	154.95 ± 12.04	90–125	1.66 ± 0.08	6.39 ± 0.24	2.91 ± 0.08	10 ± 5	0.23	3.64 ± 0.24	42.59 ± 4.37
SLK-270-274	**22**	**59.88 ± 3.45**	**90–125**	**3.14 ± 0.11**	**9.73 ± 0.29**	**2.20 ± 0.08**	**5 ± 2.5**	**0.22**	**3.78 ± 0.17**	**15.86 ± 1.15**
SLK320-324	24	138.16 ± 9.59	90–125	2.87 ± 0.11	10.40 ± 0.30	2.08 ± 0.08	10 ± 5	0.2	3.41 ± 0.24	40.49 ± 3.98

The data rendered in bold are reliable OSL ages used for chronology.

bleached before deposition. However, most aliquots of D_es of the other six fluvial samples SLK-36-40, SLK-92-96, SLK-160-164, SLK-216-220, SLK-256-260, and SLK-320-324 were scattered outside the ±2 standard deviation bands in the radial plot, indicating that the grain sizes of these samples were poorly bleached or/and unbleached before deposition. Weighted mean D_e and average standard deviations were used to estimate well bleached samples for age calculation, and ages of 6.4 ± 0.4 ka, 8.3 ± 0.4 ka and 15.7 ± 1.2 ka were obtained for samples SLK-126-130, SLK-190-194 and SLK-270-274, respectively.

One of the main problems in OSL dating of geological deposits concerns the completeness of accumulated luminescence signal reset at the moment of burial. It is assumed that for some types of sediments, such a reset is stimulated by exposure to daylight, which takes place prior to deposition. However, the effectiveness of such optical bleaching is controlled by many conditions, which strongly depend on the environment of transport and sedimentation (Przegiętka and Chruścińska, 2013). The partial bleaching of sediment not only increases the scatter of the obtained OSL results, but also makes the calculated age of the deposit appear to be older than it really is (Rittenour, 2008; Rodnight, 2008; Sun et al., 2010). To check how much the age can be affected by poor bleaching, the ages of the poorly bleached fluvial samples in SLK section were also calculated. These calculated OSL ages of 10.9 ± 0.9,

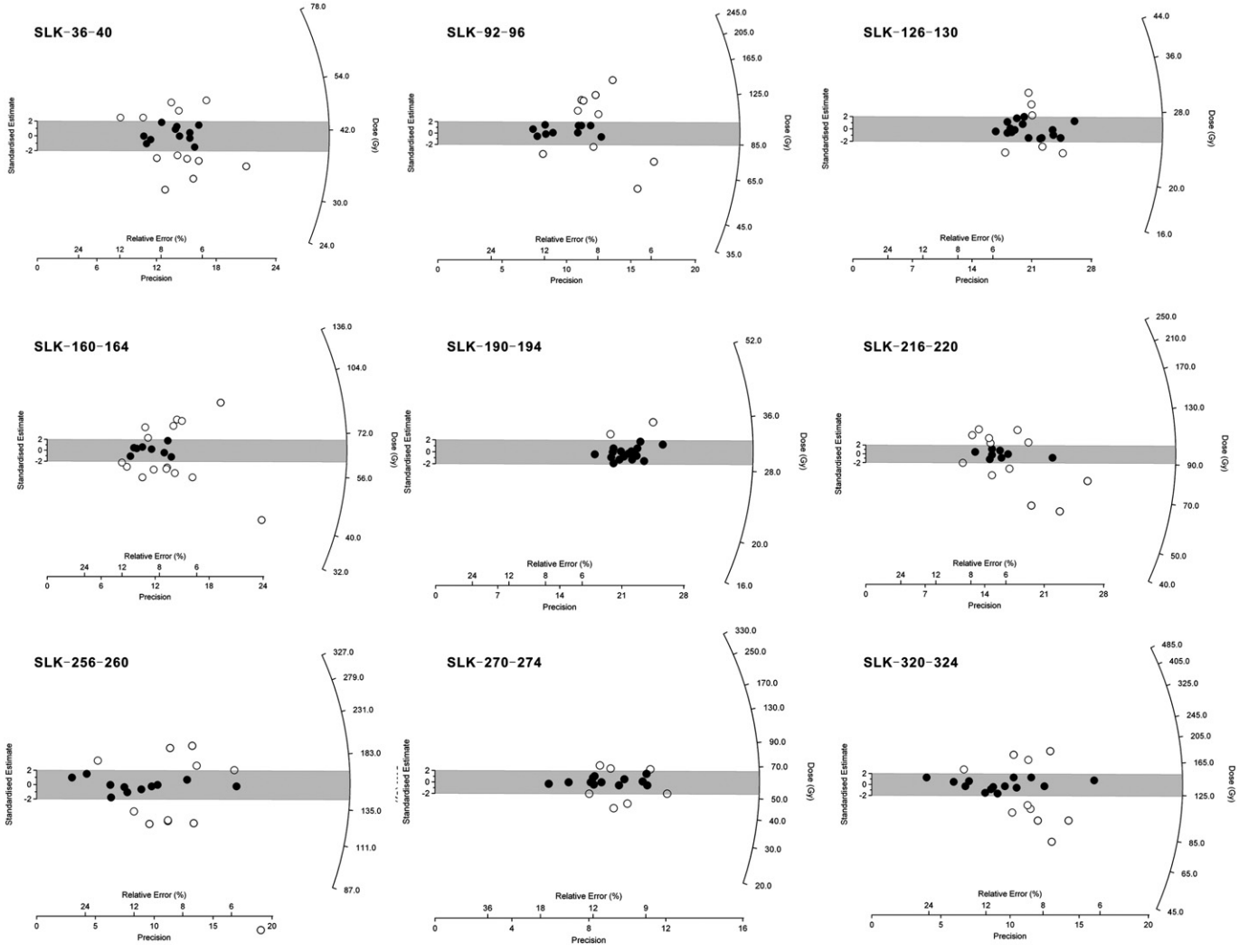

Figure 5. The distribution of D_e values in radial plots for samples SLK-36-40, SLK-92-96, SLK-126-130, SLK-160-164, SLK-190-194, SLK-216-220, SLK256-260, SLK-270-274, and SLK320-324.

https://doi.org/10.1016/j.yqres.2014.07.005 Published online by Cambridge University Press

Table 2
Calibrated radiocarbon dates for the SLK site.

Lab no.	Depth (cm)	Method	Dating material	^{14}C age (BP)	Cal yr BP 1σ (IntCal09)	Cal yr BP 2σ (IntCal09)	Reference
SLK-01	10	LQC	Charcoal	2883 ± 53	3032 ± 105	3037 ± 169	This paper
SLK-02	115	LQC	BOM	4755 ± 61	5459 ± 126	5459 ± 136	This paper
SLK-03	180	LQC	BOM	6910 ± 60	7747 ± 71	7772 ± 150	This paper
SLK-04	190	LQC	Charcoal	7535 ± 58	8317 ± 92	8310 ± 112	Dong et al. (2013a)
SLK-05	190	AMS	Charcoal	7220 ± 40	8061 ± 90	8061 ± 99	Dong et al. (2013a)

LQC—liquid scintillation counting; BOM—bulk organic matter.

28.4 ± 2.7, 18.0 ± 1.6, 26.6 ± 2.4, 42.6 ± 4.4 and 40.5 ± 4.0 ka for samples SLK-36-40, SLK-92-96, SLK-160-164, SLK-216-220, SLK-256-260, and SLK-320-324, are more than 100% overestimated compared to independent ^{14}C ages and reliable eolian OSL sample ages. This suggests that the effectiveness of optical bleaching for fluvial or water-laid deposits must be carefully examined when using OSL dating technology.

^{14}C dating results

Results of radiocarbon dating are shown in Table 2. The calibrated radiocarbon dates of SLK-01, SLK-02, SLK-03, SLK-04, and SLK-05 are 3032 ± 105, 5459 ± 126, 7747 ± 71, 8061 ± 90 and 8317 ± 93 cal yr BP, respectively. The ^{14}C ages at the bottom of unit 3 are 8061 ± 90 and 8317 ± 93 cal yr BP, and are consistent with the OSL age of 8.3 ± 0.4 ka at the same position. The ^{14}C age of sample from 110 cm unit 3 is 5459 ± 126 cal yr BP and the OSL age of the sample from 126 to 130 cm of unit 3 is 6.4 ± 0.4 ka, which, again, are consistent relative to depth. The comparison between OSL dating results and ^{14}C dating results indicate that of the OSL ages and ^{14}C ages are reliable chronological estimates. The OSL ages of 6.4 ± 0.4, 8.3 ± 0.4 and 15.9 ± 1.2 ka at the depths of 160 cm, 190 cm and 270 cm, and ^{14}C ages of 3032 ± 105, 5459 ± 126, 7747 ± 71, 8061 ± 90 and 8317 ± 93 cal yr BP at depths of 10, 110, 120, 180 and 190 cm are considered acceptable and are employed for the chronology of the SLK site.

Variations of grain size, magnetic susceptibility and color reflectance

Changes with depth in grain size, magnetic susceptibility and color reflectance of the SLK section are shown in Figure 3. Silty sand/sand dominates the bottom of the SLK section from 330 to 200 cm, with high mean grain-size fluctuations from 91 to 670 μm (lithological unit 2). Up section, the grain size decreases to a mean grain size less than 200 μm, with moderate fluctuations varying from 38 to 200 μm from 112 cm to 200 cm (lithological unit 3). The upper part of the section from 112 to 10 cm (lithological unit 4) consists of silty sand and sand with mean grain-size fluctuations from 38 to 542 μm, similar to lithological unit 2.

The magnetic susceptibility (χ_{lf}) in units 2 and 4 varies between 8 and $35 \cdot 10^{-9}$ m^3/kg and 8 and $46 \cdot 10^{-9}$ m^3/kg, while a high value of χ_{lf} appears in unit 3 ranging from 22 to $136 \cdot 10^{-9}$ m^3/kg. An χ_{lf} peak appears at the bottom of unit 2 and is as high as $136 \cdot 10^{-9}$ m^3/kg. The frequency-dependent magnetic susceptibility (χ_{fd}) generally has similar changes to χ_{lf} in the section. The χ_{fd} in unit 2 and unit 4 is generally low ranging from −2 to 7% and −3 to 6%, while in unit 3 the χ_{fd} varies from 5 to 12%.

Lightness and redness appear consistent in the section and show an opposite correlation with χ_{lf}. All samples from the SLK section have positive values ranging from 2 to 7%, and lightness ranges from 58 to 67%. Among the three units, unit 3 is characterized by low lightness (as low as 58%) and redness (as low as 2%). The highest lightness and redness values appears at the bottom of unit 3 from 150 to 200 cm.

Discussion

Paleoenvironment recorded by SLK section

Four main units in the SLK section can be reconstructed from the sediment lithology and proxy indexes analysis (Fig. 3).

Unit 1 consists of sandy pebbles or gravels, associated with the second terrace of the Yellow River that formed ~40 ka ago (Miao et al., 2012). Although the age of the sandy gravels have not been directly obtained in this study, the OSL age of the paleosol above the gravels is 15.9 ± 1.2 ka, indicating that the second Yellow River terrace in the Qunjian Basin area formed sometime prior to that time.

The grain-size frequency distributions of samples from units 2a, 2b, and 2c show three peaks, a distinctive peak at around 400 μm and two smooth peaks at around 10 μm and 60 μm (Fig. 6, unit 2). This is a typical grain-size distribution for overbank fluvial sediments of Yellow River in the SLK site area (Qiang et al., 2006; Yin et al., 2009; Chen et al., 2013). The grain size of unit 2 is silty sand, with a dramatic fluctuation in mean grain size from 100 to 700 μm, indicating that flooding frequently occurred in unit 2. The magnetism parameter (e.g., χ_{lf} and χ_{fd}) and color reflectance can be used to distinguish between sediments deposited during flooding episodes and during less frequent flooding intervals, as magnetic minerals will increase during the pedogenic process (Zhan and Xie, 2001; Shi, 2007). Magnetic minerals are sparse in the fluvial brown-red silty sand, but higher in the black eolian sandy silt. There is a color contrast between the black eolian sandy silt and the brown-red silty sand, with the values of redness and lightness being relatively higher in the latter. As shown in Figure 3, the generally low values of χ_{fd} and χ_{lf}, and the high values of redness and lightness imply a fluvial environment in unit 2. However, the redness and lightness of the sandy silt in unit 2b is at their lowest points in unit 2 and the χ_{fd} values are relatively high, indicating that the pedogenic process occurred at unit 2b. These indicators suggest that unit 2 mainly consists of overbank flow deposits of the Yellow River, but that a pedogenic process occurred during a period of river regression corresponding to unit 2b.

The grain size of unit 3 is sandy silt, and the mean grain size rapidly decreases to less than 100 μm from the bottom to top of this unit (Fig. 3, unit 3), while the clay and silt components increase. The grain-size frequency distributions of samples from unit 3, unlike the typical grain-size frequency distribution of Yellow River fluvial samples from unit 2, are characterized by smooth peaks at around 10, 40 and 600 μm. The redness and lightness values of the sandy silt in unit 3 decreased compared to those in unit 2, while χ_{lf} and χ_{fd} values rapidly increased, a shift resulting from a change from brown fluvial silty sand to black eolian sandy silt as a result of pedogenic processes. A plateau peak of χ_{lf} values and the lowest values of redness and lightness occur in the culture layer at the bottom of unit 3, again indicating soil development within this unit. Human activity may have been responsible for an increase in magnetic minerals, and thus an increase in χ_{lf} values. This unit is mainly eolian sandy silt with some soil development, and was probably deposited at a period when the Yellow River was at low water levels and overbank flow was limited. In other word, this was a non-flooding or very low-frequency flooding period.

The grain size of unit 4 consists of silty sand with interbedded sandy silt, and clay and silt trend to decrease from bottom to top. As shown in Figure 6, the grain-size frequency distributions of samples from units 4a and 4b are similar in character to unit 2, consisting of a distinctive peak at around 500 μm and two very smooth peaks at around 10 μm and 60 μm, although a few samples are characterized by one very smooth

https://doi.org/10.1016/j.yqres.2014.07.005 Published online by Cambridge University Press

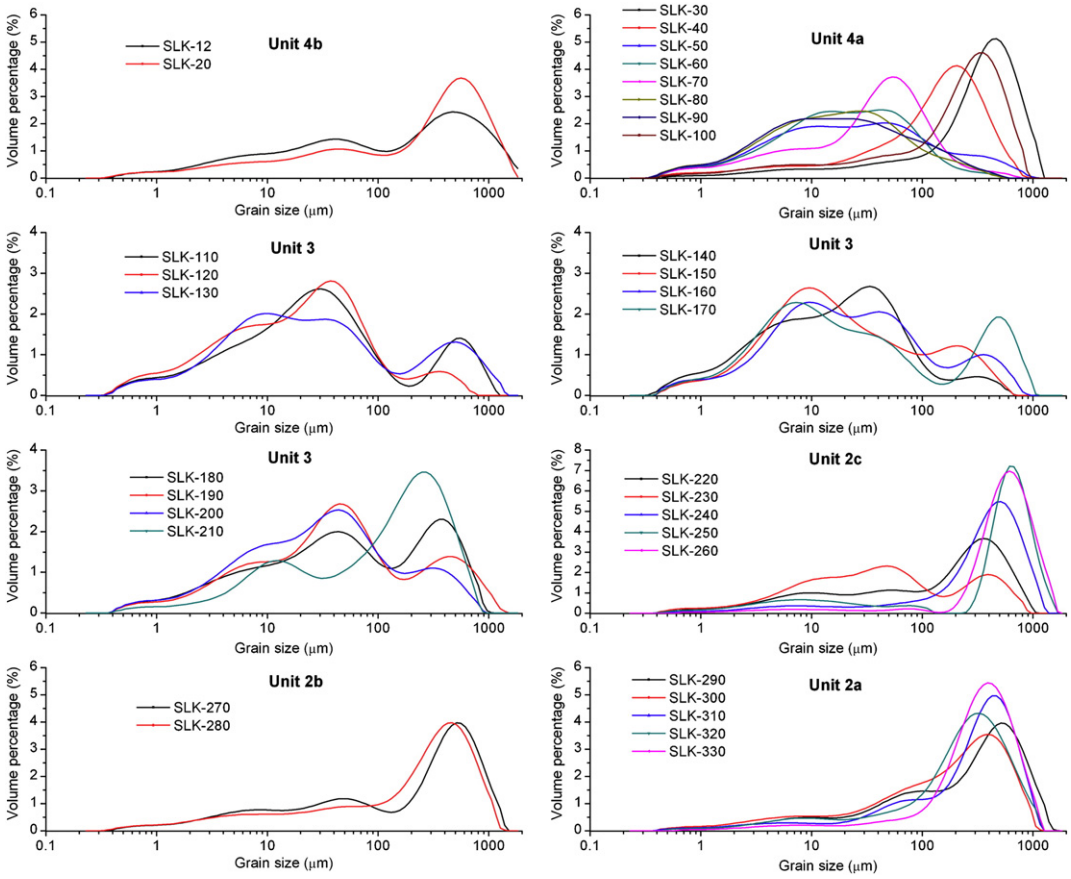

Figure 6. Grain-size frequency distribution curves for samples from different units of the SLK section.

peak at around 20 μm (Fig. 6). The redness and lightness of this unit are higher compared to unit 3, and the χ_{lf} and χ_{fd} of this unit decrease to levels similar to unit 2. All this evidence indicates that flooding occurred frequently in this unit and fluvial deposition reappeared. The modern soil developed in unit 4a is characterized by low redness and lightness, as well as high χ_{lf} and χ_{fd} values. However, the grain size of unit 4a has a typical fluvial grain-size frequency distribution, indicating that the modern pedogenic process probably occurred in fluvial deposits near the surface.

Yellow River overflow and human settlement in the SLK site area

As indicated by the SLK section, fluvial silty sand and gravelly sand deposited above the second Yellow River terrace indicates that Yellow River overbank flow occurred after the second terrace formed. The OSL age of the paleosol layer (unit 2b, Fig. 3) within the fluvial silty sand and gravel sand (unit 2a, 2c, Fig. 3) is ~16 ka, indicating that the Yellow River overflowed to its second terrace before 16 ka and that a reduction of overbank flow occurred at ~16 ka. The exact timing of second terrace formation remains unclear and needs further study.

As shown in Figure 3, the sand component of samples in unit 2c gradually decreases, and silt and clay components increases from bottom to top, indicating that water energy gradually became weaker and reduced overbank flow. The low χ_{lf} and χ_{fd} values of unit 2 suggest that no obvious pedogenic process developed on the fluvial unit 2. A rapid mean grain size decrease from unit 2 to unit 3 occurs, and mean grain size is steady around 100 μm in unit 3. The grain-size frequency curve of one distinctive peak in unit 2 changes to three smooth peaks in unit 3. The χ_{lf} and χ_{fd} values increase rapidly from unit 2 to unit 3 and a distinct peak occurs in the culture layer at the bottom of unit 3, indicating that a pedogenic process occurred in eolian sandy silt of unit 3 without flooding. It is reasonable to conclude that from unit 2 to unit 3 the fluvial and/or frequent flooding environment changed to an eolian environment without flooding or with low-frequency flooding.

The OSL age of the soil at the bottom of unit 3 is about 8.3 ka, and the ^{14}C age of charcoal from culture layer in the bottom of unit 3 is ~8.3 ka cal yr BP, indicating that Yellow River overbank flow largely stopped after ~8.3 ka and that a paleosol developed on the river overbank plain after that time. In the SLK site, microlithic artifacts are present at the bottom of unit 3 and no pottery or other Neolithic remains were found (Dong et al., 2013a). The ^{14}C ages of charcoal from the culture layer and the OSL age from the paleosol show that this culture layer formed at ~8.3 ka. Previous study at this site suggested that microlithic hunter-gatherers were present in the Qunjian Basin 8300–8150 cal yr BP (Dong et al., 2013a), an age range consistent with this study.

Sand-tempered brown and gray simple cord-marked sherds found on the ground surface of the SLK site have characteristics of early Majiayao culture. These Neolithic farmers began to settle in the upper Yellow River valley beginning ~5500 cal yr BP (Dong et al., 2013a). The calibrated ^{14}C age of bulk organic material from the paleosol at 115 cm depth in the profile is ~5450 cal yr BP, corresponding to the radiocarbon dates of charcoals from the Andaqiha Majiayao site that is just 150 m to the SLK site (Dong et al., 2013a), suggesting that the site was occupied by early Majiayao peoples when the paleosol developed. The ages of the paleosol from bottom to top in unit 3 are ~8.3 ka (OSL age), ~7700 cal yr BP (^{14}C dating age), and ~6.4 ka (OSL age), and it is reasonable to deduce that the paleosol developed during 8.3–5.4 ka. On the surface near the SLK section, a Kayue cultural layer containing an array of sand-tempered brown pottery sherds and charcoal was found. The

https://doi.org/10.1016/j.yqres.2014.07.005 Published online by Cambridge University Press

calibrated ^{14}C age of charcoal from the culture layer 10 cm below the surface is about 3030 cal yr BP, indicating that a paleosol again developed at ~3.0 ka after the Yellow River flow was reduced.

In summary, the paleosol/fluvial sequence implies that the Yellow River overbank flow intensity changed episodically. The Yellow River overflowed to its second terrace and reached the SLK site by at least ~16 ka ago, and frequent flooding periods and infrequent flooding episodes alternated until after ~3 ka. Limited flooding and associated soil formation occurred at ~15, 8.3–5.4, and ~3.0 ka, while prehistoric people occupied the SLK site area at ~8.3 ka, ~5.4 ka and ~3.0 ka,

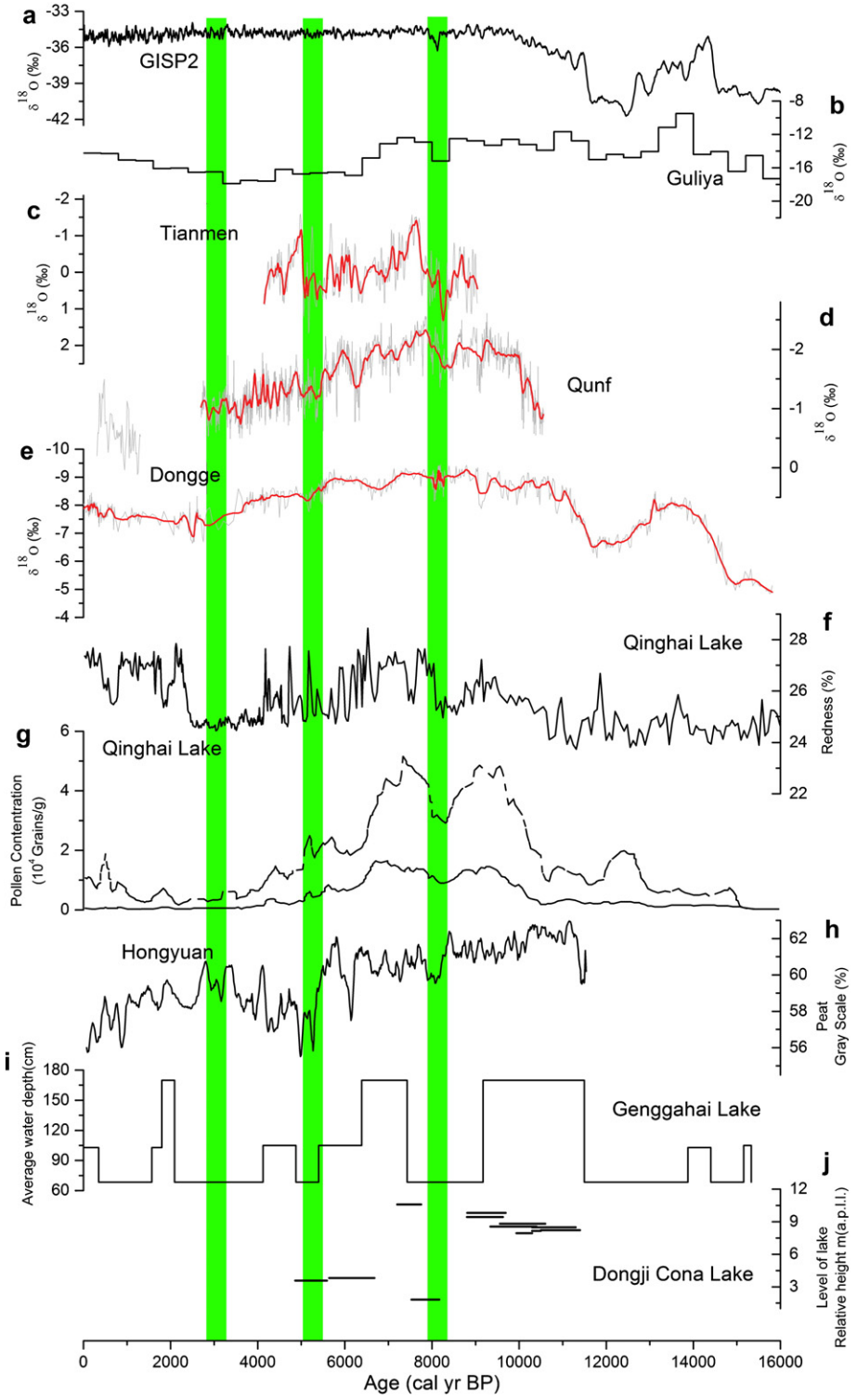

Figure 7. Comparison of human settlement at site SLK to climatic records: a — GISP2 ice core, Greenland (Stuiver et al., 1995); b — Guoliya ice core, TP (Thompson et al., 1997); c — Tianmen Cave, TP (Cai et al., 2012); d — Qunf Cave, Oman (Fleitmann et al., 2003); e — Dongge Cave D4, China (Dykoski et al., 2005); f & g — Qinghai Lake (Ji et al., 2005; Shen et al., 2005); h — Hongyuan peat land (Yu et al., 2006); i — Genggahai Lake (Qiang et al., 2013); and j — DongjiCona Lake (Dietze et al., 2013). The locations are shown in Fig. 1A. The green lines represent episodes of human settlement at the SLK site.

https://doi.org/10.1016/j.yqres.2014.07.005 Published online by Cambridge University Press

corresponding to periods of late Upper Paleolithic, early Majiayao and Kayue culture settlement.

Correlation between human occupation and climate change

During the early Holocene, people occupied the SLK site at ~8.3 ka, corresponding to a cold/dry period identified at around 8.2 ka on the TP (Liu et al., 2002; Ji et al., 2005). That cold period at around 8.2 ka was of global extent and apparently had a world-wide climatic impact (Alley et al., 1997; Cheng et al., 2009). As shown in Figs. 7a, b, e, the ~8.2 ka cold event is clearly recorded by oxygen isotope data in the GISP2 ice core in Greenland (Stuiver et al., 1995), in the Guliya ice core from the TP (Thompson et al., 1997), and in the Dongge Cave speleothem record from southern China (Dykoski et al., 2005). The $\delta^{18}O$ in precipitation has been suggested to have a quantitative correlation with air temperature on the TP and peak cooling (~8.3–8.2 ka) on the TP was ~7.8–10°C, with 3–4°C temperature decrease (Wang et al., 2002a). The speleothem oxygen isotope record from Tianmen Cave (Fig. 7c) on the southern TP and Qunf Cave (Fig. 7d) in Oman also shows that the lowest Holocene precipitation period occurred at ~8.2 ka, indicating a weak East Asia Summer Monsoon (ESM) that may have occurred in response to a Northern Hemisphere summer insolation decline during the early to mid-Holocene (Cai et al., 2012). The redness and lightness records of lake sediments from Qinghai Lake, are also considered to be indicators of precipitation, and thus, of increasing monsoon strength (Ji et al., 2005). As shown in Figure 7f, the redness at ~8.2 ka also peaks in the early middle Holocene. Pollen data from Qinghai Lake (Fig. 7g) also show a rapid decrease in arboreal pollen concentration at ~8.2 ka. All these data indicate that precipitation and temperature decreased in phase at ~8.2 ka on the TP as a result of a decrease in ESM strength. The Yellow River originates from the east-central TP, and its water sources are streams recharged by local precipitation in response to ESM, and by snow/ice melt that responded to temperature changes. Due to dry and cold climatic condition ~8.2 ka, Yellow River water flow in these source areas decreased and Yellow River overbank flow at the SLK site was correspondingly reduced. Soil development and vegetation cover may provide suitable conditions for site occupation.

The early Majiayao and Kayue cultural occupations were present in the SLK site area at ~5.4 and ~3.0 ka, respectively, both also fall in cold and dry periods on the TP. Precipitation during the middle Holocene on the TP, as indicated by $\delta^{18}O$ data from the Tianmen Cave speleothem was markedly reduced during 5.5–5 ka. The Hongyuan peat record from the southern TP, as shown in Figure 7h, also shows a marked decrease in precipitation after ~6.0 ka, with the lowest precipitation occurring ~5.4–5.0 ka. In the nearby Qinghai Lake sediment record many centennial-scale oscillations during the mid-Holocene make it difficult to confirm moist changes at ~5.4 ka from a redness curve alone. However, arboreal pollen in the sediments is much reduced during ~6–5 ka, suggesting a decrease in moisture during this period (Liu et al., 2002). Qinghai Lake lacustrine redness and pollen analyses suggest that climate conditions at ~3 ka were cold and semi-arid and arboreal pollen disappeared (Liu et al., 2002; Ji et al., 2005). The Guliya ice-core record suggests that ~3 ka temperatures on the TP decreased to their lowest levels during the whole of the Holocene (Fig. 7).

As shown in Figure 1A, Genggahai and DongjiCona lakes are near the headwaters of the Yellow River near the SLK site and lake levels at the lakes appear to have responded to ESM variability. In combination with sediment geochemical variables including TOC, TN, and $\delta^{13}C$ bulk-organic, macrofossil assemblages (aquatic plant remains, stem encrustations, and mollusc shells), Qiang et al. (2013) reconstruct lake-level fluctuations of Genggahai Lake over the past 16 ka as shown in Figure 7i. The lake sustained a low level from 9.2 to 7.4 cal ka BP during the early Holocene. Stepwise drops in lake level occurred from 6.3 to 5.5 cal ka BP, and reached their lowest level at ~5 ka with another low level lasting from 4.1 to 2.1 cal ka BP during middle-late Holocene. As shown in Figure 7j, similar low lake-level periods have been reported for DongjiCona Lake by using radiocarbon dating and grain-size analysis on the lacustrine sediment in three onshore terraces around the lake (Dietze et al., 2013). All three episodes of cultural activity at ~8.3, ~5.4 and ~3.0 ka at the SLK site fall in the low water-level intervals at Dongji Cona, indicating weak ESM periods with relatively low precipitation and temperature.

Majiayao and Kayue settlements at the SLK site occurred during periods of "harsh" climatic conditions, but flooding frequency was low during these periods and site occupants were able to avoid a natural disaster (e.g., flooding). Perhaps more importantly, millet cultivation was an important subsistence strategy during Majiayao periods (Jia et al., 2013), and millet agriculture has strict water and temperature requirements (Guedes et al., 2013; Jia et al., 2013). During periods of higher temperature and precipitation, these early millet farmers may have been able to settle far away from the river channel, but when the temperature decreased millet cultivation may have been limited in the piedmont and mountain areas, forcing people into lower elevation river valleys for millet cultivation where there were warmer conditions and a sufficient water supply. Analysis of tool assembles from excavated sites of the Majiayao culture suggests that hunting was an important auxiliary subsistence strategy (Dong et al., 2013b) and ready access to both riverine and adjacent mountain resource areas may have been another factor in the occupation of the SLK site during Majiayao period. During Kayue period, millet agriculture was still a very important subsistence strategy, while wheat and barley were also cultivated in the sites near the main channel of the Upper Yellow River (Jia, 2012), suggesting that Kayue people settled in the SLK site mainly for the convenience of obtaining water resources to guarantee food production. In summary, climatic changes might have reduced the frequency of Yellow River floods at Shalongka site area during these periods of early Majiayao and Kayue, which also prompted Majiayao and Kayue human to settle in SLK site for taking advantage of periods of fluvial stability in river valleys, as they could easily obtain water resource as well as stable and fertile lands.

Conclusion

OSL dating technology was applied to 9 samples from fluvial sandy silt, paleosol layers and culture layers. Our internal checks of the quartz OSL dating indicate that the quartz single-aliquot regenerative-dose protocol is appropriate for equivalent dose determination. OSL ages for cultural layers and eolian paleosols appear to be reliable as confirmed by comparison to independent ^{14}C ages from culture layers, but OSL ages for fluvial silty sand appear to be overestimated due to poor bleaching prior to deposition.

The Yellow River overflowed to its second terrace and reached the SLK site by at least ~16 ka ago, with frequent periods of flooding occurring episodically until ~3 ka. Periods of reduced flood frequency associated with soil development occurred at ~15, ~8.3–5.4, and after ~3 ka. Prehistoric people settled in the SLK site area at ~8.3 (late Upper Paleolithic), ~5.4 (early Majiayao) and ~3 ka (Kayue). These periods correspond to cold and dry climatic conditions, suggesting that climate change influenced overbank flooding frequency in SLK site and affected human settlement by reducing overbank flooding risks and facilitating subsistence strategies, such as hunting, fishing and the planting of crops.

Acknowledgments

This study was supported by NSFC grants 41302143, 41271218, and 41101087, and 111 Program (#B06026) of Chinese State Administration of Foreign Experts Affairs. We thank Dr. Jia Xin for helping us to collect the samples.

https://doi.org/10.1016/j.yqres.2014.07.005 Published online by Cambridge University Press

References

Aitken, M.J., 1998. An Introduction to Optical Dating. Oxford University Press, Oxford, p. 359.

Aldenderfer, M.S., 2006. Modelling plateau peoples: the early human use of the world's high plateau. World Archaeology 38, 357–370.

Alley, R.B., Mayewski, P.A., Sowers, T., Stuiver, M., Taylor, K.C., Clark, P.U., 1997. Holocene climatic instability: a prominent, widespread event 8200 yr ago. Geology 25, 483–486.

Banerjee, D., Murray, A.S., Bøtter–Jensen, L., 2001. Equivalent dose estimation using a single aliquot of polymineral fine grains. Radiation Measurements 33, 73–94.

Björck, S., Hjoft, C., Ingolfsson, O., Skog, G., 1991. Radiocarbon dates from the Antarctic Peninsula region: problems and potentia1. Quarternary Proceedings 1, 55–65.

BNCR (Bureau of National Cultural Relics), 1996. Atlas of Chinese Cultural Relics-Fascicule of Qinghai Province. China Cartograghic Publishing House Press, Beijing (In Chinese).

Botzen, W.J.W., Van Den Bergh, J.C.J.M., 2009. Managing natural disaster risks in a changing climate. Environmental Hazards 8, 209–225.

Cai, Y.J., Zhang, H.W., Cheng, H., An, Z.S., Edwards, R.L., Wang, X.F., Tan, L.C., Liang, F.Y., Wang, J., 2012. The Holocene Indian monsoon variability over the southern Tibetan Plateau and its teleconnections. Earth and Planetary Science Letters 335, 135–144.

Chen, F.H., Qiang, M.R., Zhou, A.F., Xiao, S., Chen, J.H., 2013. A 2000-year dust storm record from Lake Sugan in the dust source area of arid China. Journal of Geophysical Research 118, 2149–2160. http://dx.doi.org/10.1002/jgrd.50140.

Cheng, H., Edwards, R.L., Broecker, W.S., Denton, G.H., Kong, X.G., Wang, Y.J., Zhang, R., Wang, X.F., 2009. Ice age terminations. Science 326, 248–252.

Colinan, S.M., Jones, G.A., Rubin, M., King, J.W., Peck, J.A., Orem, W.H., 1996. AMS radiocarbon analyses from Lake Baikal, Siberia: challenges of dating sediments from a large, oligotrophic lake. Quaternary Geochronology 15, 669–684.

de Moel, H., van Alphen, J., Aerts, J.C.J.H., 2009. Flood maps in Europe-methods, availability and use. Natural Hazards and Earth System Sciences 9, 289–301.

Dietze, E., Wünnemann, B., Hartmann, K., Diekmann, B., Jin, H.J., Stauch, G., Yang, S.Z., Lehmkuhl, F., 2013. Early to mid-Holocene lake high-stand sediments at Lake DonggiCona, northeastern Tibetan Plateau, China. Quaternary Research 79, 325–336.

Dong, G.H., Jia, X., Robert, E., Chen, F.H., Li, S.C., Wang, L., Cai, L.H., An, C.B., 2013a. Spatial and temporal variety of prehistoric sites and its influencing factors in the upper Yellow River valley, Qinghai Province, China. Journal of Archaeological Science 40, 2538–2546.

Dong, G.H., Wang, L., Cui, Y.F., Robert, E., Chen, F.H., 2013b. The spatiotemporal pattern of the Majiayao cultural evolution and its relation to climate change and variety of subsistence strategy during late Neolithic period in Gansu and Qinghai Provinces, northwest China. Quaternary International 316, 155–161.

Dong, G.H., Zhang, F.Y., Ma, M.M., Fan, Y.X., Wang, Z.L., Zhang, J.W., Chen, F.H., 2014. Ancient landslide-dam events in the Jishi Gorge, upper Yellow River valley, China. Quaternary Research 81, 445–451.

Dykoski, C.A., Edwards, R.L., Cheng, H., Yuan, D.X., Cai, Y.J., Zhang, M.L., Lin, Y.S., Qing, J.M., An, Z.S., Revenaugh, J., 2005. A high resolution, absolute-dated Holocene and deglacial Asian monsoon record from Dongge Cave, China. Earth and Planetary Science Letters 233, 71–86.

Fleitmann, D., Burns, S.J., Mudelsee, M., Neff, U., Kramers, J., Mangini, A., Matter, A., 2003. Holocene forcing of the Indian monsoon recorded in a stalagmite from Southern Oman. Science 300, 1737–1739.

Galbraith, R.F., Roberts, R.G., Laslett, G.M., Yoshida, H., Olley, J.M., 1999. Optical dating of single grain and multiple grains of quartz from Jinmium rock shelter, Northern Australia: part I, experimental design and statistical models. Archaeometry 41, 339–364.

Gao, H., Zhu, C., Xu, W., 2007. Environmental change and cultural response around 4200 cal. yr BP in the Yishu River Basin, Shandong. Journal of Geographical Sciences 17, 285–292.

Guedes, J., Lu, H.L., Li, Y.X., Spengler, R., Wu, X.H., Aldenderfer, M., 2013. Moving agriculture onto the Tibetan plateau: the archaeobotanical evidence. Archaeological and Anthropological Sciences. http://dx.doi.org/10.1007/s12520-013-0153-4.

Han, W.X., Yu, L.P., Lai, Z.P., Madsen, D., Yang, S.L., 2014. The earliest well-dated archaeological site in the hyper-arid Tarim Basin and its implications for prehistoric human migration and climatic changes. Quaternary Research 82, 66–72.

Hou, G.L., Lai, Z.P., Sun, Y.J., Ye, M.L., 2012. Luminescence and radiocarbon chronologies for the Xindian Culture site of Lamafeng in the Guanting Basin on the NE edge of the Tibetan Plateau. Quaternary Geochronology 10, 394–398.

Huang, C.C., Pang, J.L., Zha, X.C., Zhou, Y.L., Su, H.X., Li, Y.Q., 2010. Extraordinary floods of 4100–4000 a BP recorded at the late Neolithic ruins in the Jinghe River gorges, middle reach of the Yellow River, China. Palaeogeography, Palaeoclimatology, Palaeoecology 289, 1–9.

IPCC, 2012. Managing the Risks of Extreme Events and Disasters to Advance Climate Change Adaptation. In: Field, C.B., et al. (Eds.), Cambridge Univ. Press.

Ji, J.F., Shen, J., Balsam, W., Chen, J., Liu, L.W., Liu, X.Q., 2005. Asian monsoon oscillations in the northeastern Qinghai-Tibet Plateau since the late glacial as interpreted from visible reflectance of Qinghai Lake sediments. Earth and Planetary Science Letters 233, 61–70.

Jia, X., 2012. Cultural Evolution Process and Plant Remains During Neolithic-bronze Age in Northeast Qinghai Province(PhD thesis) Lanzhou University, Lanzhou (in Chinese).

Jia, X., Dong, G., Li, H., Brunson, K., Chen, F., Ma, M., Wang, H., An, C., Zhang, K., 2013. The development of agriculture and its impact on cultural expansion during the mid-late Neolithic in the western loess plateau, China. The Holocene 23, 83–90.

Kidder, T.R., Liu, H.W., Li, M.L., 2012a. Sanyangzhuang: early farming and a Han settlement preserved beneath Yellow River flood deposits. Antiquity 86, 30–47.

Kidder, T.R., Liu, H.W., Xu, Q.H., Li, M.L., 2012b. The alluvial geoarchaeology of the Sanyangzhuang site on the Yellow River Floodplain, Henan Province, China. Geoarchaeology 27, 324–343.

Lai, Z.P., Kaiser, K., Brückner, H., 2009. Luminescence dated aeolian deposits of late Quaternary age in the southern Tibetan Plateau and their implications for landscape history. Quaternary Research 72, 421–430.

Lai, Z.P., Mischke, S., Madsen, D., 2014. Paleoenvironmental implications of new OSL dates on the formation of the "Shell Bar" in the Qaidam Basin, northeastern Qinghai–Tibetan Plateau. Journal of Paleolimnology 51, 197–210.

Li, S.H., Chen, Y.Y., Li, B., Sun, J.M., Yang, L.R., 2007. OSL dating of sediments from deserts in northern China. Quaternary Geochronology 2, 23–28.

Liu, X.Q., Shen, J., Wang, S.M., Yang, X.D., Tong, G.B., Zhang, E.L., 2002. A 16000-year pollen record of Qinghai Lake and its paleoclimate and paleoenvironment. Chinese Science Bulletin 47, 1931–1936.

Ma, M.M., Dong, G.H., Chen, F.H., Meng, X.M., Wang, Z.L., Elston, R., Li, G.Q., 2014. Process of paleofloods in Guanting basin, Qinghai Province, China and possible relation to monsoon strength during the mid-Holocene. Quaternary International 321, 88–96.

Markey, B.G., Bøtter-Jensen, L., Duller, G.A.T., 1997. A new flexible system for measuring thermally and optically stimulated luminescence. Radiation Measurements 27, 83–89.

Miao, Q., Qian, F., Zhao, Z.Z., Liu, X.G., 2012. Terraces and evolution of the Yellow River in the Guide Segment. Geological Survey and Research 35, 34–38 (In Chinese with English abstract).

Milly, P.C.D., Wetherald, R.T., Dunne, K.A., Delworth, T.L., 2002. Increasing risk of great floods in a changing climate. Nature 415, 514–517.

Min, S.-K., Zhang, X.B., Zwiers, F.W., Hegerl, G.C., 2011. Human contribution to more-intense precipitation extremes. Nature 470, 378–381.

Murray, A.S., Wintle, A.G., 2000. Luminescence dating of quartz using an improved single aliquot regenerative dose protocol. Radiation Measurements 32, 57–73.

Murray, A.S., Wintle, A.G., 2003. The single aliquot regenerative dose protocol: potential for improvements in reliability. Radiation Measurements 37, 377–381.

Pall, P., Aina, T., Stone, D.A., Stott, P.A., Nozawa, T., Hilberts, A.G.J., Lohmann, D., Allen, M.R., 2011. Anthropogenic greenhouse gas contribution to flood risk in England and Wales in autumn 2000. Nature 470, 382–385.

Peng, Y.J., Xiao, J.L., Nakamura, T., Liu, B.L., Inouchi, Y., 2005. Holocene East Asian monsoonal precipitation pattern revealed by grain size distribution of core sediments of Daihai Lake in Inner Mongolia of north-central China. Earth and Planetary Science Letters 233, 467–479.

Prescott, J.R., Hutton, J.T., 1994. Cosmic ray contributions to dose rates for luminescence and ESR dating: large depths and long-term time variations. Radiation Measurements 23, 497–500.

Przegiętka, K.R., Chruścińska, A., 2013. Analysis of optical bleaching of OSL signal in sediment quartz. Radiation Measurements 56, 257–261.

Qiang, M.R., Chen, F.H., Zhang, J.W., Zu, R.P., Jin, M., Zhou, A.F., Xiao, S., 2006. Grain size in sediments from Lake Sugan: a possible linkage to dust storm events at the northern margin of the Qinghai–Tibetan Plateau. Environmental Geology 51, 1229–1238.

Qiang, M.R., Song, L., Chen, F.H., Li, M.Z., Liu, X.X., Wang, Q., 2013. A 16-ka lake-level record inferred from macrofossils in a sediment core from Genggahai Lake, northeastern Qinghai–Tibetan Plateau (China). Journal of Paleolimnology 49, 575–590.

Reimer, P.J., Baillie, M.G.L., Bard, E., Bayliss, A., Beck, J.W., Blackwell, P.G., Bronk Ramsey, C., Buck, C.E., Burr, G.S., Edwards, R.L., Friedrich, M., Guilderson, T.P., Hajdas, I., Heaton, T.J., Hogg, A.G., Hughen, K.A., Kaiser, K.F., Kromer, B., McCormac, G., Manning, S.W., Reimer, R.W., Richards, D.A., Southon, J.R., Talamo, S., Turney, C.S.M., van der Plicht, J., Weyhenmeyer, C.E., 2009. IntCal09 and Marine09 radiocarbon age calibration curves, 0–50,000 years Cal BP. Radiocarbon 51, 1111–1150.

Rittenour, T.M., 2008. Luminescence dating of fluvial deposits: applications to geomorphic, palaeoseismic and archaeological research. Boreas 37, 613–635.

Robertson, A.R., 1977. The CIE 1976 color-difference formulate. Color Research and Application 2, 7–11.

Rodnight, H., 2008. How many equivalent dose values are needed to obtain a reproducible distribution? Ancient TL 26, 3–9.

Shen, J., Liu, X.Q., Wang, S.M., Matsumoto, R., 2005. Palaeoclimatic changes in the Qinghai Lake area during the last 18,000 years. Quaternary International 136, 131–140.

Shi, X.M., 2007. Progress of research on palaeofloods. Journal of China Hydrology 27, 24–28 (in Chinese).

Stuiver, M., Reimer, P.J., 1993. Extended ^{14}C database and revised CALIB radiocarbon calibration program. Radiocarbon 35, 215–230.

Stuiver, M., Grootes, P.M., Braziunas, T.F., 1995. The GISP2 ä^{18}O climate record of the past 16500 years and the roles of the sun, ocean and volcanos. Quaternary Research 44, 341–354.

Sun, Y.J., Lai, Z.P., Long, H., Liu, X.J., Fan, Q.S., 2010. Quartz OSL dating of archaeological sites in Xiao Qaidam Lake of the NE Qinghai–Tibetan Plateau and its implications for palaeoenvironmental changes. Quaternary Geochronology 5, 360–364.

Sun, Y.J., Lai, Z.P., Madsen, D., Hou, G.L., 2012. Luminescence dating of a hearth from the archaeological site of Jiangxigou in the Qinghai Lake area of the northeastern Qinghai–Tibetan Plateau. Quaternary Geochronology 12, 107–110.

Thompson, L.G., Yao, T.D., Davis, M.E., 1997. Tropical climate instability: the last glacial cycle from a Qinghai–Tibetan ice core. Science 276, 1821–1825.

Wang, N.L., Yao, T.D., Thompson, L.G., Henderson, K.A., Davis, M.E., 2002a. Evidence for cold events in the early Holocene from Guliya ice core, TP, China. Chinese Science Bulletin 47, 1422–1427.

Wang, R.L., Scarpitta, S.C., Zhang, S.C., Zheng, M.P., 2002b. Later Pleistocene/Holocene climate conditions of Qinghai—Xizang Plateau (Tibet) based on carbon and oxygen

https://doi.org/10.1016/j.yqres.2014.07.005 Published online by Cambridge University Press

stable isotopes of Zabuye Lake sediments. Earth and Planetary Science Letters 203, 461–477.
Wang, Y., Chan, H., Edwards, R.L., He, Y., Kong, X., An, Z., Wu, J., Kelly, M.G., Dykoski, C.A., 2005. The Holocene Asian monsoon: links to solar changes and North Atlantic climate. Science 308, 854–857.
Wilby, R.L., Beven, K.J., Reynard, N.S., 2008. Climate change and fluvial flood risk in the UK: more of the same? Hydrological Processes 22, 2511–2523.
Yang, D., Yu, G., Xie, Y., Zhan, D., Li, Z., 2000. Sedimentary records of large Holocene floods from the middle reaches of the Yellow River, China. Geomorphology 33, 73–88.
Yang, X.Y., Xia, Z.K., Ye, M.L., 2003. Prehistoric disasters at Lajia site, Qinghai, China. Chinese Science Bulletin 48, 1877–1881.
Yin, Z.Q., Qin, X.G., Wu, J.S., Ning, B., 2009. The multimodal grain-size distribution characteristics of loess, desert, lake and river sediment in some areas of northern China. Acta Sedimentologica Sinica 27, 343–351 (in Chinese with English abstract).
YRCC (Yellow River Conservancy Commission), 1959. The People's Yellow River. Water Resources and Electric Power Press, Beijing (in Chinese).
Yu, L.P., Lai, Z.P., 2014. Holocene climate change inferred from stratigraphy and OSL chronology of aeolian sediments in the Qaidam Basin, northeastern Qinghai–Tibetan Plateau. Quaternary Research 81, 488–499.
Yu, X.F., Zhou, W.J., Franzen, Lars G., Xian, F., Cheng, P., Tim Jull, A.J., 2006. High-resolution peat records for Holocene monsoon history in the eastern Tibetan Plateau. Science in China Series D: Earth Sciences 49, 615–621.
Zhan, D.J., Xie, Y.B., 2001. Palaeoflood Study. China Water Power Press, Beijing (in Chinese).
Zhang, J.F., Zhou, L.P., 2007. Optimization of the 'double SAR' procedure for polymineral fine grains. Radiation Measurements 42, 1475–1482.
Zhang, J.F., Liu, C.L., Wu, X.H., Liu, K.X., Zhou, L.P., 2012. Optically stimulated luminescence and radiocarbon dating of sediments from Lop Nur (LopNor), China. Quaternary Geochronology 10, 150–155.
Zhao, H., Chen, F.-H., Li, S.-H., Wintle, A.G., Fan, Y.X., Xia, D.S., 2007. A record of Holocene climate change in the Guanzhong Basin, China. The Holocene 17, 1015–1022.
Zhao, H., Li, G.-Q., Sheng, Y.-W., Jin, M., Chen, F.H., 2012. Early-middle Holocene Paleolake-desert evolution in northern Ulan-Buh desert, China. Palaeogeography Palaeoclimatology Palaeoecology 331–332, 31–38.

https://doi.org/10.1016/j.yqres.2014.07.005 Published online by Cambridge University Press